Influence of the nonresonant processes in the dynamics of the image-potential states of Cu(100) and Ag(100)

Y. J. Dappe and A. A. Villaeys
Institut de Physique et Chimie des Matériaux de Strasbourg, 23 rue du Loess, 67037 Strasbourg Cedex, France
(Received 12 February 2003; published 20 June 2003)

We will concentrate on the peculiar role played by the nonresonant processes resulting from the existence of an initial distribution of bulk states on the two-photon photoemission spectroscopy of Cu(100) and Ag(100) surfaces. In contrast to previous studies on the Cu(111) surface where the process is initiated from an intrinsic surface state, here the transitions occur between the initially occupied bulk band states located below the energetic gap and the image-potential states because there is no intrinsic surface state for this type of surface orientation. We will show that the initial distribution of bulk states plays an important role in the evolution of the image-potential states and cannot be reduced to a single state as previously described. The resulting nonresonant processes can strongly affect the magnitude of the resonance structure of the photoemission spectrum with respect to the predictions obtained on the basis of the sole resonant process.

DOI: 10.1103/PhysRevB.67.235415 PACS number(s): 73.20.−r, 79.60.Bm, 78.47.+p

I. INTRODUCTION

Image-potential states are now well-established as states where the surface electron is trapped due to the Coulombic interaction with its image charge located in the metal.[1] Because these states are generally unoccupied, their experimental detection and identification have been realized first through inverse photoemission spectroscopy.[2–4] Then, the observation of low-lying image-potential states was carried out these last decades for different metal surfaces.[5] The description of the surface electron moving freely parallel to the surface and trapped perpendicular to the surface has been conveniently given in terms of plane waves along the uncorrugated surface times hydrogenic *s* wave functions along the normal to the surface. There has been strong emphasis on the determination of the image-potential state lifetimes accessible by two-photon photoemission spectroscopy,[6–8] and the influence of adsorbate layers of rare gases deposited on the bulk has been studied.[9–11] In addition, some general rules based on the experimental observations give a quantitative relation $\tau_n \propto p_n^{-1}$ between the lifetime τ_n of the image-potential state and its penetration factor p_n corresponding to the modulus squared of the surface wave function restricted to its *z* dependence and integrated over the bulk.[12]

While these observations were first performed by taking advantage of the energy resolution, the high time resolution attainable today with femtosecond lasers in two-photon photoemission (2PPE) spectroscopy offers the opportunity to follow in real time ultrafast dynamics occurring among image-potential states, intrinsic surface states or bulk states, and photoemitted electron states.[7,9,13,14] The first measurement on the determination of the 2PPE spectra was carried out on Ag(100) and Ag(111) using uv-pump–ir-probe delayed pulses and showed the emergence of the second image-potential state during the rapid decay of the first one.[15,16] The experimental determination of the cross-correlation curves $n=1$ and $n=0$ performed on the Cu(111) surface by time-resolved 2PPE spectroscopy has attracted much attention.[9,13] The origin of the process underlying the $n=1$ cross-correlation curve as resulting from a simple sequential population process initiated from the intrinsic surface state through the intermediate image-potential state was well understood. However, the case of the cross-correlation curve $n=0$ was a subject of controversy. It is now clear that it results from a purely coherent process where a population of extracted photoelectrons is created through coherences among the initial intrinsic surface state, the intermediate image-potential state, and the final photoelectron state. This interpretation is confirmed by the location of the energy of the surface electron resonances corresponding to $n=0$ and $n=1$.[17,18] Of course, not all the metallic surfaces have intrinsic surface states participating in the photoemission process, such as Cu(111). This is particularly true for the (100) surface of copper and silver studied recently by Shumay *et al.*,[7] where the time-resolved two-photon photoemission process is initiated from the bulk band states. Starting from a supercell geometry, Klamroth, Saalfrank, and Höfer[19] have used a mapped Fourier-grid Hamiltonian method to simulate such an experiment by introducing the local effective one-electron potential of Chulkov, Silkin, and Echenique[20] using a multistate open-system density matrix approach. They gave a description of the pump-probe process including energy and phase relaxation that enables evaluation of the energy- and time-resolved 2PPE signal. This work is based on a generic *ab initio* type of approach to avoid the introduction of any idealized scaling law about energies and lifetimes of the image-potential states. By solving the eigenvalue problem numerically and the dynamics of a multistate open-density matrix model including continua of initial and final states, Chulkov, Silkin, and Echenique simulate the time-resolved 2PPE spectra. Although the method is quite powerful and enables the evaluation of the image-potential states up to $n=15$, the numerical predictions compared to the experimental 2PPE signal underestimate the $n=1$ resonance while it overestimates the $n=2$, resonance as mentioned by the authors.

It is the goal of this work to show that a similar difficulty can be encountered in evaluating analytically the 2PPE spec-

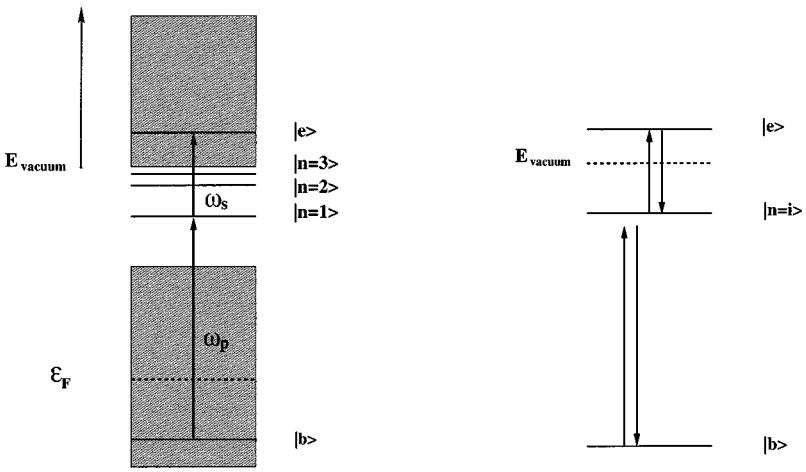

FIG. 1. On the left-hand side of the figure, we represent the electronic structure of Cu(100) and Ag(100) surfaces, involving bulk band states, image-potential states, as well as the continuum of photoemitted electron states. On the right-hand side, the sequential population process leading to the extraction of the photoemitted electron through the intermediate image potential state $n=i$ is illustrated.

tra of the image-potential states when the sole resonant contributions are retained. Of course, because the initial and the final state distributions pertain to two continua, we are always faced with competition between resonant and nonresonant contributions. For this reason, it can be tempting, as done in previous work, to reduce the dynamics to the sole states contributing to the resonant transitions. We will demonstrate that such an oversimplified model would lead to an erroneous evaluation of the spectra due to the high sensitivity of the 2PPE spectrum with the density of initial states or, equivalently, to the nonresonant processes.

II. RESONANT APPROACH TO THE DYNAMICS OF IMAGE-POTENTIAL STATES

2PPE spectroscopy is mainly described in terms of the sole resonant processes which usually gives the main contributions to the signal intensity detected in these experiments. Then, time-dependent or energy-dependent calculations are carried out to simulate the cross-correlation functions or the spectra of the photoemitted electrons. Basically, the description is done in terms of the dynamical equations obtained from the Liouville equation of the density matrix $\rho(t)$,

$$\frac{\partial\rho(t)}{\partial t}=-\frac{i}{\hbar}[H_0+V(t),\rho(t)]-\Gamma\rho(t), \tag{2.1}$$

of the surface system interacting with the pump and probe pulsed fields described microscopically in the semiclassical approach, assuming the dipolar approximation. Therefore the interaction terms can be expressed as

$$V(t)=-\sum_{v=p,s}\boldsymbol{\mu}\cdot[\mathbf{E}(\Omega_v)e^{-i\Omega_v t}+\text{c.c.}]e^{-\gamma_r|t-\bar{t}_v|}. \tag{2.2}$$

Here, $\boldsymbol{\mu}$ is the usual dipole moment operator that needs to be considered for the particular transition involved in the process. It interacts with the electric field of the biexponential laser pulse, $\bar{t}_v$ being the pumping or the probing time and γ_v^{-1} the duration of the pump or the probe pulse, depending on whether $v=p$ or s, respectively. The quantity $\mathbf{E}(\Omega_v)$ stands for the amplitude of the pulse at frequency Ω_v. Notice that the analytical structure of the pulse shape adopted in the present work has negligible consequences on the physical results due to time integration. For the problem at hand, the area and the width of the pulse are important. More realistic envelopes will be probably described by Gaussian shapes, impeding an analytical treatment. However, the pulse durations must be much shorter than the dynamical times of the electronic system; otherwise they affect the dynamical evolution and must be accounted for in the analysis of the experimental results. This is the case we are dealing with in the present study, because the pump and probe pulse durations are even longer than the lifetimes or dephasing times of the system. This is why the pulse shape enters in our description.

Finally, relaxation and dephasing processes occurring between surface electron states or surface and bulk electron states are accounted for by the damping Liouvillian operator Γ. For our present purpose, the two surface systems of interest are the Cu(100) and Ag(100) surfaces. These two metallic surfaces share the fact that the two-photon photoemission processes are initiated from an occupied bulk state below the energy level because there is no intrinsic surface state for these surfaces. The electronic structure associated with both surfaces can be schematically represented as shown on Fig. 1, where the sequential process responsible for the photoemission is indicated. Therefore, the corresponding Hamiltonian driving the surface dynamics in these 2PPE experiments is usually restricted to a three-level system

$$H_0=E_b|b\rangle\langle b|+E_i|i\rangle\langle i|+E_e|e\rangle\langle e|, \tag{2.3}$$

where $|b\rangle$, $|i\rangle$, and $|e\rangle$ stand for the bulk state, the image potential state and the photoelectron state, respectively. Therefore, the inelastic and elastic processes taking place during the course of the experiments will be accounted for by dephasing constants Γ_{bibi}, total decay rates Γ_{iiii} and Γ_{bbbb}, transition rate Γ_{bbii}, and the various pure dephasing constants $\Gamma_{bi}^{(d)}$, $\Gamma_{be}^{(d)}$, and $\Gamma_{ie}^{(d)}$. All the other constants are negligible and this is particularly true for the lifetime of the photoelectron state. In addition, all these quantities are related by the expression $\Gamma_{ijij}=\frac{1}{2}[\Gamma_{iiii}+\Gamma_{jjjj}]+\Gamma_{ij}^{(d)}$ for the dephasing constants and sum rules for the transition constants and total decay rates.

We focus on the $n=1$, $n=2$, and $n=3$ resonances of the image-potential states of the Cu(100) and Ag(100) surfaces. Therefore the underlying dynamical process is clearly identified as a sequential population process.[17] This process arises due to the population created in the image-potential state from the initial bulk state by the femtosecond pump pulse and subsequently excited by the probe pulse to extract electrons from the surface. Here, we have no intrinsic surface state, and there is no observation of resonant structure in the electronic spectra resulting from a possible coherent contribution. The photoemitted electron population created by the pulses from the bulk band states through the image-potential state is evaluated for weak light beams by a fourth-order perturbation expansion with respect to $V(t)$. Therefore, the formal expression for the population of photoemitted electrons is given by

$$\rho_{ee}^{(4)}(t)=\frac{1}{\hbar^4}\sum_{m,n,p,q,r,u}\int_{t_0}^{t}dt_4\int_{t_0}^{t_4}dt_3\int_{t_0}^{t_3}dt_2 \times\int_{t_0}^{t_2}dt_1 G_{eeee}(t-t_4)L_{eeur}^{V}(t_4) \times G_{urur}(t_4-t_3)L_{urqp}^{V}(t_3)G_{qpqp}(t_3-t_2) \times L_{qpnm}^{V}(t_2)G_{nmnm}(t_2-t_1)L_{nmbb}^{V}(t_1)\rho_{bb}(t_0), \tag{2.4}$$

where $\rho_{bb}(t_0)=1$ with the system completely relaxed at the initial time t_0 implying $G_{bbbb}(t_1-t_0)\equiv 1$. The various contributions are associated to the combinations of indices shown in the following table:

m	n	p	q	r	u
b	i	i	i	i	e
b	i	i	i	e	i
i	b	i	i	i	e
i	b	i	i	e	i

Here, the main difficulty lies on the analytical structure of the laser pulse envelopes, which has been overcome in a previous study of pumped sum-frequency generation involving five-wave mixing processes.[21] Here, $L^V(t)=[V(t),\ ]$ is the interaction Liouvillian and $G(t'-t'')=\exp[-(i/\hbar)(L-i\hbar\Gamma)(t'-t'')]$ stands for the free evolution Liouvillian. Their matrix elements are quite often expressed in terms of their spectral decompositions obtained in the Liouvillian eigenstate basis set. For our system, these states satisfy the eigenvalue problem

$$\left[-\frac{i}{\hbar}L-\Gamma\right]|\alpha\alpha\rangle\rangle=\mathcal{E}_\alpha|\alpha\alpha\rangle\rangle,\quad \alpha=1,2,3. \tag{2.5}$$

The evaluation of $G_{ijij}(t-t')$ for the coherences is straightforward because Γ is diagonal in the Liouvillian subspace of the coherences so that

$$G_{ijij}(t-t')=e^{-i\omega_{\widehat{ij}}(t-t')-\Gamma_{\widehat{ijij}}(t-t')},\quad i\neq j. \tag{2.6}$$

However, the spectral decomposition $G_{iijj}(t-t')$ for the population is more intricate due to the presence of the transition constants and requires the diagonalization of the zero-order Liouvillian in the population subspace.[21] In the particular case of our three-level system, we obtain

$$\mathcal{E}_1=0,\quad \mathcal{E}_2=\Gamma_{bbbb}+\Gamma_{iiii},\quad \mathcal{E}_3=0, \tag{2.7}$$

with the corresponding overlapings

$$\begin{aligned}\langle\langle ee|33\rangle\rangle\langle\langle 33|ee\rangle\rangle&=1,\\ \langle\langle ii|11\rangle\rangle\langle\langle 11|ii\rangle\rangle&=\langle\langle bb|22\rangle\rangle\langle\langle 22|bb\rangle\rangle\\ &=\Gamma_{bbbb}/(\Gamma_{bbbb}+\Gamma_{iiii}),\\ \langle\langle ii|22\rangle\rangle\langle\langle 22|ii\rangle\rangle&=\langle\langle bb|11\rangle\rangle\langle\langle 11|bb\rangle\rangle\\ &=\Gamma_{iiii}/(\Gamma_{bbbb}+\Gamma_{iiii}).\end{aligned} \tag{2.8}$$

Therefore, the evolution of the population is given by

$$G_{iijj}(t-t')=\sum_{\vartheta}\langle\langle ii|\vartheta\vartheta\rangle\rangle e^{-r_\vartheta(t-t')}\langle\langle\vartheta\vartheta|jj\rangle\rangle\quad\forall\ (i,j), \tag{2.9}$$

where, for our system,

$$\begin{aligned}G_{iiii}(t-t')&=\frac{1}{\Gamma_{bbbb}+\Gamma_{iiii}}[\Gamma_{bbbb}+\Gamma_{iiii}e^{-(\Gamma_{bbbb}+\Gamma_{iiii})(t-t')}],\\ G_{eeee}(t-t')&=1.\end{aligned} \tag{2.10}$$

From the expressions of these matrix elements the determination of the surface electron population $\rho_{ee}^{(4)}(t)$ is readily evaluated.

The five-wave mixing process quite generally reproduces the two-photon photoemission process in which the extraction of a surface electron is substituted by the emission of the coherent signal. Here, in contrast, only two different probing times $\overline{t_p}$ and $\overline{t_s}$ exist because the electronic population is dependent on the interaction of the sample with both the pump pulse and the probe pulse. Therefore, the evaluation of the population of extracted electrons results from contributions of the different pathways η described previously having the general form

$$\int_{t_0}^{t}\int_{t_0}^{t_4}\int_{t_0}^{t_3}\int_{t_0}^{t_2}dt_4\cdots dt_1 e^{D_\eta t_4+C_\eta t_3+B_\eta t_2+A_\eta t_1}e^{-\gamma_s|t_4-\overline{t_s}|-\gamma_s|t_3-\overline{t_s}|-\gamma_p|t_2-\overline{t_p}|-\gamma_p|t_1-\overline{t_p}|} \tag{2.11}$$

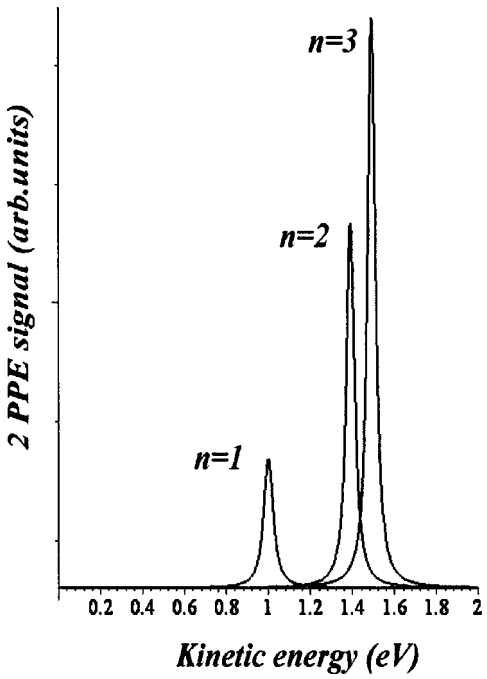

FIG. 2. Variations of the 2PPE signal intensities obtained from our model by retaining the sole resonant contribution. The initial bulk state is chosen to assume resonant condition between the pump field frequency and the transition between bulk state and image-potential state.

and only the constants of pathways 1 and 2 will be evaluated, because the others can be deduced by simple complex conjugation. Notice that if the argument of the exponential cancels, the limit has to be taken properly. Since we are interested in the determination of the number of electrons ejected from the surface at a given energy and in a given direction, we only require the probability at long times. This probability is obtained as follows. The expression of $\rho_{ee}^{(4)}(t)$ is obtained by multiple time integration. We reject from this expression the exponential time-dependent terms that go to zero in the limit $t\rightarrow\infty$ because their arguments are strictly negative. Otherwise, their contributions must be retained. Finally, the number of electrons that have been photoemitted through the sequential process at long times is a function of $\overline{t_s}-\overline{t_p}$ and corresponds to

$$N(\overline{t_s}-\overline{t_p})=\lim_{t\rightarrow\infty}\rho_{ee}^{(4)}(t), \tag{2.12}$$

where the detailed expression is presented in the Appendix. As an example, we simulate in Fig. 2, the 2PPE spectrum of the Cu(100) surface using the numerical values taken from the experiments performed by Shumay *et al.*[7] The pump laser beam has been chosen to be resonant with the bulk and image-potential state transition. The electronic 2PPE spectrum exhibits three resonances associated with the image-potential states $n=1$, 2, and 3. While the location of the energies of these resonances is correct, we observe a complete inversion of their magnitudes with respect to the experimental data, showing that the resonance $n=1$ is smaller than $n=2$, and itself is smaller than $n=3$. We will demonstrate in the following that this discrepancy arises from the fact that we have rejected the nonresonant contributions in this preliminary description. This point will be considered in the next section.

III. INFLUENCE OF THE INITIAL BULK STATE DISTRIBUTION

For the present purposes, a number of experimental data concerning both the laser pulses and the electronic surface system are required. Since we are dealing with the two-photon photoemission spectra performed by Shumay *et al.*, the parameters of the excitation pulses are taken from Ref. 7. To perform the simulations emphasizing the role of the nonresonant process, the physical parameters characterizing the energy levels corresponding to the particular cases of the Cu(100) and Ag(100) surfaces are required. They are modelized by the general formula

$$E_n=-\frac{\mathcal{R}}{16(n+a)^2}, \tag{3.1}$$

at $\mathbf{k}_{\|}=\mathbf{0}$ and with a the quantum defect of the corresponding surface and $\mathcal{R}$ the Rydberg constant. These energies fit the experimental measurements obtained from these surfaces quite well.[22] Also, the vacuum level energy is required. All these data are given below.

To illustrate our purpose and stress the influence of the nonresonant contributions, we still need the coupling parameters. For the sake of simplicity, we first assume that all the couplings are comparable. Later, we will discuss the particular case of the surfaces of interest here. There is a continuous distribution of initial bulk states that, at least in principle, can participate in the sequential photoemission process. Of course, for a given pump laser beam frequency, besides the resonant contribution provided by the bulk state associated with the resonant excitation of the image-potential state, all the other bulk states contribute nonresonantly to the photoemission spectrum. While nonresonant contributions are generally quite small with respect to the resonant ones, we will show in this section that the nonresonant contributions associated with the continuous distribution of initial bulk states modify substantially the spectrum of the image-potential states obtained in a 2PPE experiment for the different image-potential states. Taking into account the continuous distribution of initial bulk states, the cross-correlation function as well as the photoemission spectrum must now be summed over the initial distribution and can be obtained from

$$N(\overline{t_s}-\overline{t_p},E_{\mathrm{kin}})=\int dE_b\sigma(E_b)\rho_{ee}^{(4)}(t\rightarrow\infty), \tag{3.2}$$

where $\sigma(E_b)$ represents the density of initial bulk states.

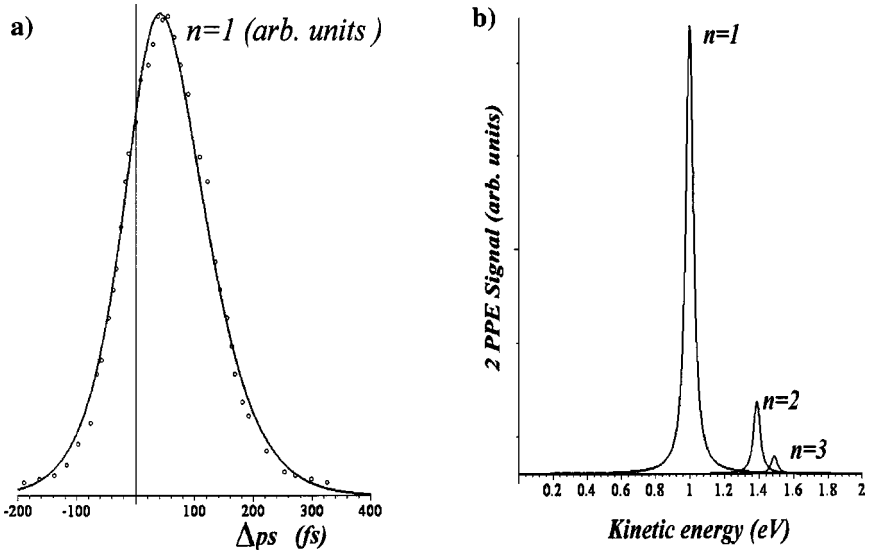

FIG. 3. We fit the experimental 2PPE signal intensity versus the pump-probe delay time obtained by Shumay *et al.* (Ref. 7) for the $n=1$ resonance of the Cu(100) surface. From the evaluation of the dynamical constants obtained for $n=1$ and the measured lifetimes of the image-potential states $n=2$ and 3, the spectra of the photoemitted electron versus their kinetic energies have been determined for these image potential states.

Since the distribution of initial states is specific from the bulk, these are similar for the three resonances and will not affect the relative contributions of the 2PPE resonance spectra. Therefore, we have chosen a simple uniform distribution. It is interesting to note that the introduction of an initial distribution of states has previously been introduced by Klamroth, Saalfrank, and Höfer in a different approach.[19]

Besides the determination of the dynamical constants, we want to emphasize the high sensitivity of the surface electron spectra of Cu(100) and Ag(100) to the nonresonant processes that can take place during the course of a 2PPE experiment. Both 2PPE spectroscopy experiments performed on Cu(100) and Ag(100) surfaces present some similarities because none of these surfaces have an occupied intrinsic surface state lying below the Fermi level. Therefore, the sequential process leading to the photoemission process starts, in both cases, from an initial distribution of the bulk state, enabling a unified description of these experiments. Also, both experiments have been realized with uv-pump and ir-probe laser beams at energies of $\hbar\omega_p = 4.71$ eV and $\hbar\omega_s = 1.57$ eV, with pulse durations of 90 and 70 fs, respectively. For the particular case of the Cu(100) surface, the vacuum energy is $E_{\text{vacuum}} = 4.63$ eV, and the various image-potential state energies are, at $\mathbf{k}_{\parallel} = \mathbf{0}$, $E_1 = 4.06$ eV, $E_2 = 4.45$ eV, and $E_3 = 4.55$ eV for the three first image-potential states $n=1$, 2, and 3, respectively. All the energies are defined with respect to the Fermi level.

The time- and energy-dependent cross-correlation curves obtained by 2PPE spectroscopy are represented on Fig. 3. By introducing a continuous distribution of bulk states, we have evaluated the cross-correlation function to fit the experimental data obtained for $n=1$ on the Cu(100) surface. It gives the values $\Gamma_{1111}^{-1} = 35.7$ fs, $\Gamma_{1b}^{(d)^{-1}} = 20$ fs, $\Gamma_{1e}^{(d)^{-1}} = 200$ fs, and $\Gamma_{be}^{(d)^{-1}} = 50$ fs. Notice that the value of the image-potential state lifetime has to be compared to that of 40 fs obtained by Shumay *et al.*, by neglecting the influence of the duration of the pulsed excitation, which is far from being negligible in their experiment.

In addition, from these simulations, we observe that the influence of the pure dephasing constants $\Gamma_{1b}^{(d)}$ and $\Gamma_{eb}^{(d)}$ is quite weak on the 2PPE spectrum. Taking advantage of these

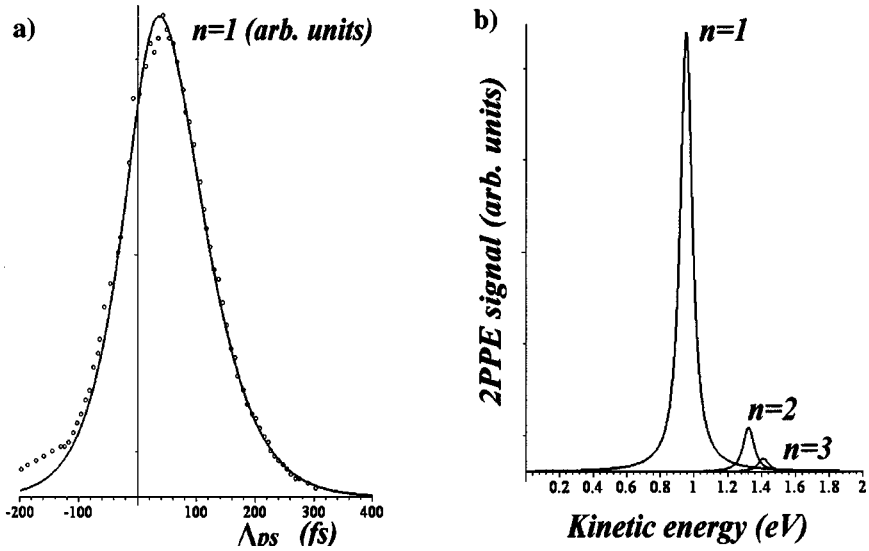

FIG. 4. As done in the previous figure, we fit the experimental 2PPE signal intensity versus the pump-probe delay time obtained by Shumay *et al.* (Ref. 7) for the $n=1$ resonance of the Ag(100) surface. Again, on the right side of the figure, by using the values of the dynamical constants, we similarly reproduce the spectra of the photoemitted electron as a function of their kinetic energies for the image potential states $n=1$, 2, and 3.

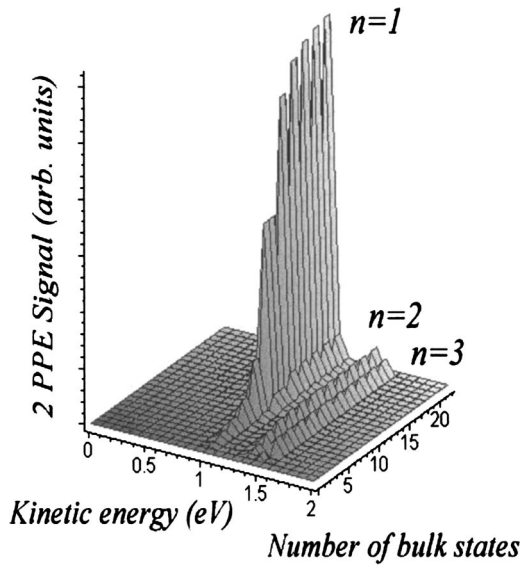

FIG. 5. We analyze the relative magnitudes of the various resonances $n=1$, 2, and 3, as a function of the number of initial bulk states contributing to the nonresonant transitions. We observe a complete inversion of the peak sizes for increasing values of the number of bulk states.

physical parameters the 2PPE spectral distribution of the photoemitted electrons has been evaluated as a function of the kinetic electron energy given by $E_c=\hbar\omega_s-(E_{\text{vacuum}}-E_1)$. Because of the lack of experimental data on the cross-correlation functions for $n=2$ and 3, the 2PPE spectral distributions for these two last image-potential states have been obtained using the energies and total decay rates obtained from the experiment of Shumay *et al.* Their spectra are drawn in the same figure together with $n=1$. We recover the correct ratio for the peak intensities of the three resonances. A similar evaluation has been done for the Ag(100) surface. The corresponding cross-correlation function and the spectra are represented in Fig. 4. Again, the cross-correlation function for the image-potential state $n=1$, as well as the spectra associated with the three first image-potential states $n=1$, 2, and 3, has been obtained. The lifetime is now $\Gamma_{1111}^{-1}=43.5$ fs versus 55 fs, while the dephasing constant corresponds to $\Gamma_{1b}^{(d)^{-1}}=20$ fs, $\Gamma_{1e}^{(d)^{-1}}=20$ fs, and $\Gamma_{be}^{(d)^{-1}}=50$ fs. To illustrate the importance of the density of initial bulk states on the peak ratio of the various resonances, we have drawn the photoemitted spectra as a function of the electron kinetic energy for different numbers of initial bulk states. This is shown in the Fig. 5, where the underestimation of the resonances associated with the first image-potential states is stressed. We see that increasing the number of initial bulk states results in the increase of the resonances $n=1$ and 2 at the expense of the resonance $n=3$. Notice that the simulation has been done for numerical values of the parameters corresponding to the case of the Cu(100) surface.

It is interesting to note that Klamroth, Saalfrank, and Höfer[19] have recently analyzed the experimentally energy-resolved 2PPE signals at zero delay time between pump and probe pulses with respect to both the full dissipation model and the wave-packet model. From their analysis, it appears that the theoretical evaluation leads to an underestimation of the resonance $n=1$ with respect to $n=2$, even if the resonance peak for $n=1$ is nevertheless higher then that of $n=2$. In fact, in their approach, the distribution of the initial bulk states is accounted for by averaging over 17 bulk states. It seems to us that the discrepancies of the $n=1$ peak size arise from an underestimation of the number of initial bulk states since, as we can see from our simulation on Fig. 5, for the peak sizes of the resonances have not reach the limiting values for this amount of initial bulk states. Therefore, these results obtain by Klamroth, Saalfrank, and Höfer confirm our observation of high sensitivity of the photoemitted resonance structure with the distribution of initial bulk states. Finally, we want to mention that similar evaluations can be made from the phenomenological coupling structure $|\boldsymbol{\mu}|\sim(n+a)^{-3/2}$ used by Klamroth, Saalfrank, and Höfer and initially introduced by Höfer *et al.*[6] While this analytical dependence tends to reduce the relative size of the peak resonances, the effect is still present.

IV. CONCLUSION

In this work, we have emphasized the high sensitivity of the two-photon photoemission spectrum with the density of initial bulk states. Starting from a single bulk state, we have shown that the magnitude of the various resonances can be completely inverted if we increase the bulk state density. This clearly demonstrates that besides the resonant contribution participating in the 2PPE process, all the initially populated bulk states participating in the population of the image-potential state through nonresonnant transitions play an important role and contribute efficiently to the photoemitted electron spectra. This result suggests that a proper determination of the relative contributions to the various resonances associated with the different image-potential states $n=1$, 2, and 3, has to be done carefully. It requires a precise evaluation of the distribution of bulk states participating in the photoemission process. While the particular cases of the Cu(100) and Ag(100) two-photon photoemission spectra have been considered here, the problem is quite general in this type of spectroscopy.

It will be interesting in the future to have more experimental information on the cross-correlation functions of the different image-potential states to correlate the magnitude of the pics to the lifetime, which is from our analysis the dominant parameter for the magnitude of these resonances.

APPENDIX

We introduce here the detailed expression of the number of detected photoelectrons:

$$N(\bar{t}_s-\bar{t}_p)=2\,\mathrm{Re}\sum_{\eta=1,2}\sum_{\vartheta,\zeta}S_\eta(\vartheta,\zeta)\Bigg\{-\sum_{\beta=1}^{5}D^{>}_{\beta\eta}e^{2\gamma_s\bar{t}_s}(C_\eta+d^{>}_{\beta\eta}-\gamma_s)^{-1}I(T^{>}_{sp},D_\eta+C_\eta+d^{>}_{\beta\eta}-2\gamma_s)$$

$$+\sum_{\beta=1}^{5}D^{>}_{\beta\eta}e^{2\gamma_s\bar{t}_s}I(T^{>}_{sp},C_\eta+d^{>}_{\beta\eta}-\gamma_s)I(T^{>}_{sp},D_\eta-\gamma_s)-D^{<}_{1\eta}I(T^{<}_{sp},C_\eta+d^{<}_{1\eta}+\gamma_s)I(\bar{t}_s,D_\eta-\gamma_s)$$

$$+D^{<}_{1\eta}e^{-2\gamma_s\bar{t}_s}I(T^{<}_{sp},C_\eta+d^{<}_{1\eta}+\gamma_s)\bar{H}(\bar{t}_s-\bar{t}_p)J(\bar{t}_s,\bar{t}_p,D_\eta+\gamma_s)+D^{<}_{1\eta}e^{-2\gamma_s\bar{t}_s}(C_\eta+d^{<}_{1\eta}+\gamma_s)^{-1}I(T^{<}_{sp},D_\eta+C_\eta$$

$$+d^{<}_{1\eta}+2\gamma_s)-D^{<}_{1\eta}e^{2\gamma_s\bar{t}_s}\bar{H}(\bar{t}_p-\bar{t}_s)J(\bar{t}_p,\bar{t}_s,C_\eta+d^{<}_{1\eta}-\gamma_s)I(T^{>}_{sp},D_\eta-\gamma_s)+D^{<}_{1\eta}e^{2\gamma_s\bar{t}_s}(C_\eta+d^{<}_{1\eta}-\gamma_s)^{-1}\bar{H}(\bar{t}_p$$

$$-\bar{t}_s)J(\bar{t}_p,\bar{t}_s,D_\eta+C_\eta+d^{<}_{1\eta}-2\gamma_s)-D^{<}_{1\eta}e^{2\gamma_s\bar{t}_s}I(\bar{t}_s,C_\eta+d^{<}_{1\eta}-\gamma_s)\bar{H}(\bar{t}_p-\bar{t}_s)J(\bar{t}_p,\bar{t}_s,D_\eta-\gamma_s)$$

$$-\sum_{\beta=1}^{5}D^{>}_{\beta\eta}\bar{H}(\bar{t}_s-\bar{t}_p)J(\bar{t}_s,\bar{t}_p,C_\eta+d^{>}_{\beta\eta}+\gamma_s)I(\bar{t}_s,D_\eta-\gamma_s)+\sum_{\beta=1}^{5}D^{>}_{\beta\eta}e^{-2\gamma_s\bar{t}_s}(C_\eta+d^{>}_{\beta\eta}+\gamma_s)^{-1}J(\bar{t}_s,\bar{t}_p,D_\eta$$

$$+C_\eta+d^{>}_{\beta\eta}+2\gamma_s)-\sum_{\beta=1}^{5}D^{>}_{\beta\eta}e^{-2\gamma_s\bar{t}_s}\bar{H}(\bar{t}_s-\bar{t}_p)I(\bar{t}_p,C_\eta+d^{>}_{\beta\eta}+\gamma_s)J(\bar{t}_s,\bar{t}_p,D_\eta+\gamma_s)\Bigg\}, \tag{A1}$$

where the auxiliary functions $I(\tau,A)=\exp(A\tau)/A$ as well as $J(\tau_1,\tau_2,A)=[\exp(A\tau_1)-\exp(A\tau_2)]/A$ have been introduced. Also, Re corresponds to the real part and the symbols $T^{>}_{sp}$ and $T^{<}_{sp}$ stand for the higher and the smaller values of $\bar{t}_p$ and $\bar{t}_s$, respectively. All the constants arising from the successive integrations are given by

$$P^{>}_{1\eta}=e^{A_\eta\bar{t}_p}/(A_\eta+\gamma_p)-e^{A_\eta\bar{t}_p}/(A_\eta-\gamma_p),\quad p^{>}_{1\eta}=0,$$

$$P^{>}_{2\eta}=e^{\gamma_p\bar{t}_p}/(A_\eta-\gamma_p),\quad p^{>}_{2\eta}=A_\eta-\gamma_p,$$

$$P^{<}_{1\eta}=e^{-\gamma_p\bar{t}_p}/(A_\eta+\gamma_p),\quad p^{<}_{1\eta}=A_\eta+\gamma_p,$$

as well as

$$D^{>}_{1\eta}=P^{<}_{1\eta}e^{-\gamma_p\bar{t}_p}I(\bar{t}_p,B_\eta+p^{<}_{1\eta}+\gamma_p),\quad d^{>}_{1\eta}=0,$$

$$D^{>}_{2\eta}=P^{>}_{1\eta}e^{\gamma_p\bar{t}_p}(B_\eta+p^{>}_{1\eta}-\gamma_p)^{-1},\quad d^{>}_{2\eta}=B_\eta+p^{>}_{1\eta}-\gamma_p,$$

$$D^{>}_{3\eta}=P^{>}_{2\eta}e^{\gamma_p\bar{t}_p}(B_\eta+p^{>}_{2\eta}-\gamma_p)^{-1},\quad d^{>}_{3\eta}=B_\eta+p^{>}_{2\eta}-\gamma_p,$$

$$D^{>}_{4\eta}=-P^{>}_{1\eta}e^{\gamma_p\bar{t}_p}I(\bar{t}_p,B_\eta+p^{>}_{1\eta}-\gamma_p),\quad d^{>}_{4\eta}=0,$$

$$D^{>}_{5\eta}=-P^{>}_{2\eta}e^{\gamma_p\bar{t}_p}I(\bar{t}_p,B_\eta+p^{>}_{2\eta}-\gamma_p),\quad d^{>}_{5\eta}=0,$$

$$D^{<}_{1\eta}=P^{<}_{1\eta}e^{-\gamma_p\bar{t}_p}(B_\eta+p^{<}_{1\eta}+\gamma_p)^{-1},\quad d^{<}_{1\eta}=B_\eta+p^{<}_{1\eta}+\gamma_p.$$

Finally, the various constants associated with the time integration (2.11) for the first and the second pathways shown on the previous table are defined below. They correspond to

$$S_1(\vartheta,\zeta)=\langle\langle ee|\vartheta\vartheta\rangle\rangle\langle\langle\vartheta\vartheta|ee\rangle\rangle\boldsymbol{\mu}_{ie}\cdot\mathbf{E}(-\Omega_s)\boldsymbol{\mu}_{ei}\cdot\mathbf{E}(\Omega_s)\langle\langle ii|\zeta\zeta\rangle\rangle\langle\langle\zeta\zeta|ii\rangle\rangle\boldsymbol{\mu}_{si}\cdot\mathbf{E}(-\Omega_p)\boldsymbol{\mu}_{is}\cdot\mathbf{E}(\Omega_p),$$

$$s_1(\vartheta,\zeta)=-r_\vartheta,$$

$$D_1(\vartheta,\zeta)=r_\vartheta+i\Omega_s-i\omega_{ei}-\Gamma_{eiei},$$

$$C_1(\vartheta,\zeta)=i\omega_{ei}+\Gamma_{eiei}-i\Omega_s-r_\zeta,$$

$$B_1(\vartheta,\zeta)=r_\zeta+i\Omega_p-i\omega_{is}-\Gamma_{\mathrm{isis}},$$

$$A_1(\vartheta,\zeta)=i\omega_{is}+\Gamma_{\mathrm{isis}}-i\Omega_p,$$

$$S_2(\vartheta,\zeta)=\langle\langle ee|\vartheta\vartheta\rangle\rangle\langle\langle\vartheta\vartheta|ee\rangle\rangle\boldsymbol{\mu}_{ei}\cdot\mathbf{E}(\Omega_s)\boldsymbol{\mu}_{ie}\cdot\mathbf{E}(-\Omega_s)\langle\langle ii|\zeta\zeta\rangle\rangle\langle\langle\zeta\zeta|ii\rangle\rangle\boldsymbol{\mu}_{si}\cdot\mathbf{E}(-\Omega_p)\boldsymbol{\mu}_{is}\cdot\mathbf{E}(\Omega_p),$$

$$s_2(\vartheta,\zeta) = -r_\vartheta,$$

$$D_2(\vartheta,\zeta) = r_\vartheta - i\Omega_s - i\omega_{ie} - \Gamma_{\text{ieie}},$$

$$C_2(\vartheta,\zeta) = i\omega_{ie} + \Gamma_{\text{ieie}} + i\Omega_s - r_\zeta,$$

$$B_2(\vartheta,\zeta) = r_\zeta + i\Omega_p - i\omega_{is} - \Gamma_{\text{isis}},$$

$$A_2(\vartheta,\zeta) = i\omega_{is} + \Gamma_{\text{isis}} - i\Omega_p. \tag{A2}$$

[1] P. Echenique and J. Pendry, J. Phys. C **11**, 2065 (1978).
[2] P. D. Johnson and N. V. Smith, Phys. Rev. B **27**, 2527 (1983).
[3] V. Dose, W. Altmann, A. Goldmann, U. Kolac, and J. Rogozik, Phys. Rev. Lett. **52**, 1919 (1984).
[4] D. Straub and F. J. Himpsel, Phys. Rev. B **33**, 2256 (1986).
[5] K. Giesen, F. Hage, F. J. Himpsel, H. J. Reiss, and W. Steinmann, Phys. Rev. Lett. **55**, 300 (1985).
[6] H. Höfer, I. L. Shumay, C. Reuß, U. Thomann, and W. Wallauer, Science **277**, 1480 (1997).
[7] I. L. Shumay, U. Höfer, C. Reuß, U. Thommann, W. Wallauer, and T. Fauster, Phys. Rev. B **58**, 13974 (1998).
[8] T. Fauster, C. Reuß, I. L. Shumay, and M. Weinelt, Chem. Phys. **251**, 111 (2000).
[9] M. Wolf, E. Knoesel, and T. Hertel, Phys. Rev. B **54**, R5295 (1996).
[10] C. B. Harris, N.-H. Ge, J. R.-L. Lingle, J.-D. McNeill, and C.-M. Wong, Annu. Rev. Phys. Chem. **48**, 711 (1997).
[11] W. Berthold, U. Höfer, P. Feulner, and D. Menzel, Chem. Phys. **251**, 123 (2000).
[12] P. M. Echenique, J. M. Pitarke, E. V. Chulkov, and A. Rubio, Chem. Phys. **251**, 1 (2000).
[13] T. Hertel, E. Knoesel, M. Wolf, and G. Ertl, Phys. Rev. Lett. **76**, 535 (1996).
[14] M. Wolf, Surf. Sci. **377/379**, 343 (1997).
[15] R. Schoenlein, J. Fujimoto, G. Eesley, and T. Capehart, Phys. Rev. Lett. **61**, 2596 (1989).
[16] R. Schoenlein, J. Fujimoto, G. Eesley, and T. Capehart, Phys. Rev. B **41**, 5436 (1990).
[17] A. A. Villaeys, Y. J. Dappe, and F. P. Lohner, Phys. Rev. B **63**, 155113 (2001).
[18] Y. J. Dappe, A. A. Villaeys, and F. P. Lohner, Appl. Surf. Sci. **168**, 41 (2000).
[19] T. Klamroth, P. Saalfrank, and U. Höfer, Phys. Rev. B **64**, 035420 (2001).
[20] E. V. Chulkov, V. M. Silkin, and P. M. Echenique, Surf. Sci. **437**, 330 (1999).
[21] A. A. Villaeys and F. P. Lohner, Phys. Rev. A **59**, 3926 (1999).
[22] L. Kleinman and J. C. Phillips, Phys. Rev. **125**, 819 (1962).